Noninvasive fingerprinting-based tracking of replicative cellular senescence using a colorimetric polyion complex array

Shunsuke Tomita,[*,†] Hiroki Nomoto,[‡] Toru Yoshitomi,[‡] Kazutoshi Iijima,[§] Mineo Hashizume,[§] Keitaro Yoshimoto[*,‡,//]

[†] Biomedical Research Institute, National Institute of Advanced Industrial Science and Technology, and DAILAB, 1-1-1 Higashi, Tsukuba, Ibaraki 305-8566, Japan.

[‡] Department of Life Sciences, Graduate School of Arts and Sciences, The University of Tokyo, 3-8-1 Komaba, Meguro, Tokyo 153-8902, Japan.

[§] Department of Industrial Chemistry, Faculty of Engineering, Tokyo University of Science, 12-1 Ichigayafunagawara-machi, Shinjuku, Tokyo 162-0826, Japan.

[//] JST, PRESTO, The University of Tokyo, Komaba 3-8-1, Meguro, Tokyo 153-8902, Japan

Supporting Information Placeholder

ABSTRACT: A fingerprint-based sensing approach was used to characterize *in vitro* cellular senescence. Secretion profiles of cultured human fibroblasts in different senescent stages were transformed into colorimetric enzyme-activity fingerprints by applying cell-culture media to a polyion complex array. Analyzing the obtained fingerprints using pattern recognition methods, such as linear discriminant analysis and hierarchical clustering analysis, revealed that the polyion complex array allows the noninvasive tracking of the replicative senescence progress even in those stages where a conventional marker such as senescence-associated β-galactosidase is negative. This fingerprint-based approach should thus offer an effective way for the routine monitoring or screening of *in vitro* cell-senescence studies.

Cellular senescence is an anti-proliferative program that limits the propagation of cells subjected to different kinds of stimuli, such as DNA damage, chromatin perturbations, activation of cancer genes, and loss of telomeres after extensive proliferation.[1] Although cellular senescence has initially been considered as an irreversible cell-cycle-arrest mechanism that acts to protect against cancer, recent discoveries have revealed that cellular senescence may also be a detrimental biological process. For example, when senescent cells are retained in tissue for prolonged periods of time, these cells promote age-related tissue dysfunction by secreting factors that recruit local inflammation, induce aberrant tissue architecture, and impair tissue homeostasis and regeneration.[2,3]

As the characterization of senescent cells *in vivo* has been limited by difficulties associated with detecting and tracking senescent cells in real tissue, most current insights regarding senescent cells have been acquired using cell-culture experiments.[3] Therefore, one of the key issues in this field is the development of methods to accurately characterize senescent cells in culture. For this purpose, a variety of senescence-associated markers,[1] especially senescence-associated β-galactosidase (SA-β-Gal),[4-7] has been employed. However, so far, the use of a combination of multiple markers is still required, as a single universal marker for cell senescence has not yet been discovered.

The secretory profile has attracted substantial attention in the context of understanding and characterizing cultured senescent cell populations, as cell senescence is accompanied by widespread changes in the secretion of proteins, including inflammatory cytokines, chemokines, growth factors, and proteases, which are known as senescence-associated secretory phenotype (SASP) or senescence-messaging secretome (SMS).[3,8] Recent comprehensive protein analyses using antibody arrays have shown that senescence inductions with a variety of stimuli have a common and significant influence on secretion profiles for dozens of selected proteins.[9-11]

We have recently proposed a sensing strategy to acquire information on secretory profiles in cell-culture media, and used it to identify normal/cancer-cell types and stem-cell-differentiation lineages.[12] This strategy was developed using a fingerprint-based sensing technique, which exploits the pattern recognition of unique fingerprints for analytes.[13] In general, fingerprints are generated with arrays of cross-reactive molecules that can interact in different ways with analytes. This technique has been employed for the detection of proteins that are solubilized in dilute solutions[14-18] or in biological matrices.[19-22] A distinct advantage of fingerprint-based sensing is that it can also be applied to recognize the composition of complex matrices themselves, such as serum[21,23,24] and cell lysate,[15,25,26] even though not all components present may be known.[27]

Similarly, our fingerprint-based sensing of the secretory profile was created without any information on the proteins secreted from the cultured cells.[12] In our approach, polyion complexes (PICs) between anionic enzymes and poly(ethylene glycol)-modified polyamines were used as cross-reactive molecules.[21,28,29] The incubation of cell-culture media with the PICs causes the release of enzymes through competitive interactions between the secreted proteins and the PICs, which generates unique fingerprints consisting of the amount of changes in enzyme activity as variates. Inspired by that work, we exploited a PIC array to recognize senescent-related secretomic profiles of normal human fibroblasts.

The current study is based on the hypothesis that the SASP production due to replicative senescence could modulate the interaction patterns between secreted proteins and individual PICs, which

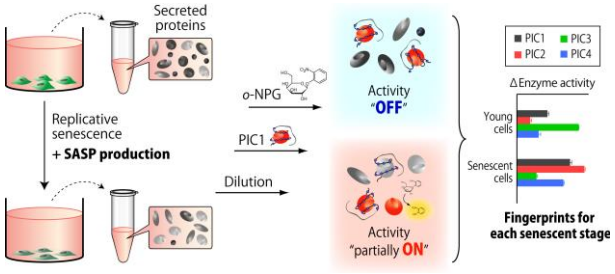

Figure 1. Schematic representation of the fingerprinting-based tracking of replicative senescence of human fibroblasts using a PIC array.

could generate enzyme-activity fingerprints that are unique to different senescent stages (Figure 1). In order to create PIC arrays that are able to generate differential fingerprints for the tracking of senescence progression, structurally diverse PICs are required. Based on our previous report,[12] we chose PICs with the following features; (i) β-galactosidase from two different sources, i.e., from *Aspergillus oryzae* (GAO, M_w = 110,000, *pI* = 5.2) and *Escherichia coli* (GEC, M_w = 465,000, *pI* = 5.1), and (ii) quaterinzed poly(ethylene glycol)-*block*-poly(*N*,*N*-dimethylaminoethyl methacrylate) (PEG-*b*-QPAMA) block co-polymers that contain functional groups with different hydrophobicity, i.e., **P1**: benzyl groups (*log P* = 2.56) and **P2**: 1-hydroxyethyl groups (*log P* = -0.40) (Figure 2A). The β-galactosidase from either source is suitable for practical use, owing to the high catalytic activity with respect to the hydrolysis of chromogenic *o*-nitrophenyl-β-D-galactopyranoside (*o*NPG) and the high structural stability.[28,29]

The addition of PEG-*b*-QPAMAs markedly decreased the catalytic activity of both enzymes against *o*NPG in 20 mM 3-(*N*-morpholino)propanesulfonic acid (MOPS) buffer (pH = 7.0) (Figure 2B) due to the electrostatically driven formation of PIC.[30,31] Consistent with a previous report,[29] hydrophobic **P1** exerted a more substantial effect on the inhibition of the enzymes.

Once the binding ratio that provided high inhibition had been determined, we investigated the capability of the PIC array to track cellular senescence. The conventional human fibroblast cell line TIG-1 was chosen, considering its extensive use as a model cell line for *in vitro* senescence studies.[32,33] According to the literature, replicative senescence was induced in TIG-1 by serial passaging.[32,33] The appearance of senescent cells was examined by the SA-β-Gal assay, i.e., a histochemical detection of the β-galactosidase activity. Although this assay may produce false-positive results under certain conditions such as confluence, it is the most widely used method due to its general applicability and simplicity.[3,4] TIG-1 did not show a positive staining for conventional SA-β-Gal assays until the increase in the population-doubling level (ΔPDL) reached 56 (Figure 3A), i.e., the point where the cells exhibited a markedly decelerated growth. Therefore, we examined the tracking of the progress of TIG-1 senescence in the SA-β-Gal-negative stages (ΔPDL = 6, 19, 34, and 46).

For the sample preparation, TIG-1 cells in different senescence stages were seeded at 4×10^4 cells/cm^2 in Dulbecco's modified Eagle's medium (DMEM) supplemented with 10% fetal bovine serum. After 16 hours of incubation, the medium was replaced with a chemically defined serum-free medium (CDCHO medium). The culture supernatants were collected after 48 hours of incubation. The obtained culture supernatants were diluted to a total protein concentration of 5 μg/mL (20 μL) and then added to individual wells of a 96-well plate, which contained solutions of PICs in 20

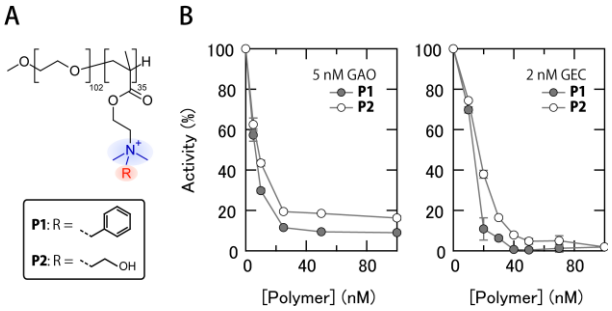

Figure 2. Changes in the enzyme activity upon addition of PEG-*b*-QPAMAs. (A) Chemical structures of the PEG-*b*-QPAMA block co-polymers. (B) Normalized enzyme activity of 5 nM GAO or 2 nM GEC for 5 mM *o*NPG with various concentrations of PEG-*b*-QPAMAs were measured in 20 mM MOPS (pH = 7.0).

mM MOPS (pH = 7.0; 100 μL; for details, see the Supporting Information). After 30 min of incubation, 25 mM *o*NPG in 20 mM MOPS (pH = 7.0; 30 μL) was added, and the enzyme activity was quantified using the time course of the absorbance at 400 nm, generating a training matrix (4 PICs × 4 ΔPDLs × 6 replicates) (Table S1).

Figure 3B shows the changes in enzyme activity for four PICs. The addition of culture supernatants resulted in increased enzyme activities, indicating that competitive interactions occurred between PICs and secreted molecules, such as proteins. In order to examine whether the individual fingerprints differ significantly, these were subjected to a linear discriminant analysis (LDA), i.e., a supervised pattern recognition method that produces a graphical data output that provides insight into data clustering.[13] In a linear discriminant score plot (Figure 4A), each point represents the fingerprint of a single analyte in the PIC array. The plot showed four separated clusters corresponding to the individual ΔPDLs in a three-dimensional space. Interestingly, the cluster positions did not

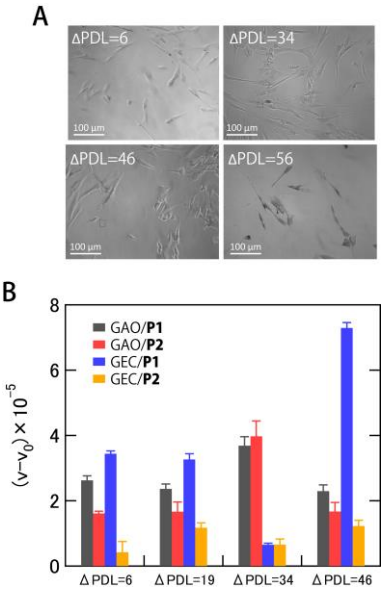

Figure 3. Fingerprinting of the secretomic profiles of TIG-1 in different senescent stages. (A) SA-β-Gal-staining of TIG-1. (B) Fingerprints of the changes in enzyme activity obtained from a PIC array. Values are shown as mean values ± SD (*n* =6).

change in a simple monotonous fashion with increasing ΔPDL, i.e., in the initial senescence stages (ΔPDL = 6-19), the cluster moves along the *z*-axis, which accounts for merely 0.4% of the total variance. After that, the cluster position varied markedly, especially on the *x*- (98.7% of the total variance) and *y*-axes (0.9% of the total variance). Thus, it seems feasible to assume that the selected PICs are probably more susceptible to the changes in secretory profiles regarding the later stages of TIG-1 senescence.

To evaluate the reliability of our sensing system to correctly identify senescence levels, a cross-validation analysis was performed. A leave-one-out procedure (jackknife classification analysis) revealed accuracies of 46-83% when using one PIC, while combinations of four PICs afforded 100% classification accuracy (Table S2). Combined, our PIC array was able to track the gradual senescence progress of TIG-1 by generating enzyme-activity fingerprints.

In order to quantitatively investigate the relevance between the response generation and the senescence progression, the distances between all analytes were visualized via an unsupervised hierarchical clustering analysis (HCA) (Figure 4B), where the calculated distance between analytes corresponds to similarities in the fingerprints of the analytes.[13] Again, four clusters corresponding to individual values of ΔPDL were well distinguished in a horizontal dendrogram, wherein ΔPDL = 19 and ΔPDL = 46 were initially clustered, followed by ΔPDL = 6 and ΔPDL = 34. For TIG-1 cells, many factors such as telomere shortening,[34] expression regulations of genes including cell cycle inhibitors,[35] mitochondria[36] and other proteins,[35,37,38] are involved in cellular senescence. In general, SASP is produced in a dynamic fashion during cellular senescence, i.e., early SASP is dominated by the secretion of the transforming growth factor-β (TGFβ) family, while subsequent signals of interleukin-1α (IL-1α) or p38-mitogen-activated protein kinase (MAPK) cause late SASP, which consists of metalloproteinases, IL-6, IL-8, and numerous other factors.[3] Consequently, about half of the analyzed 120 proteins exhibited significant differences with respect to secretory quantities between presenescent and senescent cells.[9] Therefore, our time-course analysis implies that these complicated and serial senescent-stage-dependent changes in the composition of proteins were sensed by the PIC array. Further investigations of the correlation between response fingerprints of model cells and gene/protein expression patterns at each senescent stage should provide a more detailed understanding of not only the mechanism underlying the generation of fingerprints but that of cellular senescence.

Finally, the similarities in the responses of individual PIC elements were analyzed to gain insight into the effective design of cross-reactive PIC sets. A vertical dendrogram (Figure 4B) afforded two branches that comprise i) GAO-consisting PICs, and ii) GEC-containing PICs. In other words, we observed a lower correlation between the responses generated by PICs containing different enzymes. Thus, it could be argued that the enzymes possibly play a more dominant role in the interactions with secretomic components related to senescence. Accordingly, the use of different enzymes may be effective to acquire diverse responses reflecting TIG-1 senescence. The use of block co-polymers with different functional groups that e.g. increase the hydrophobicity should lead to a further diversification of responses and improve the discrimination ability.

In summary, we have developed a proof-of-concept study for the fingerprinting-based tracking of replicative senescence of normal human fibroblasts. Significantly, this sensing system is capable of generating unique fingerprints that reflect different senescent levels, even at the stage where the most commonly used senescent marker SA-β-Gal is negative. In contrast to the conventional specific marker-based methods, this fingerprint-based approach enables the characterization of cultured cells based on the "overall" secretion

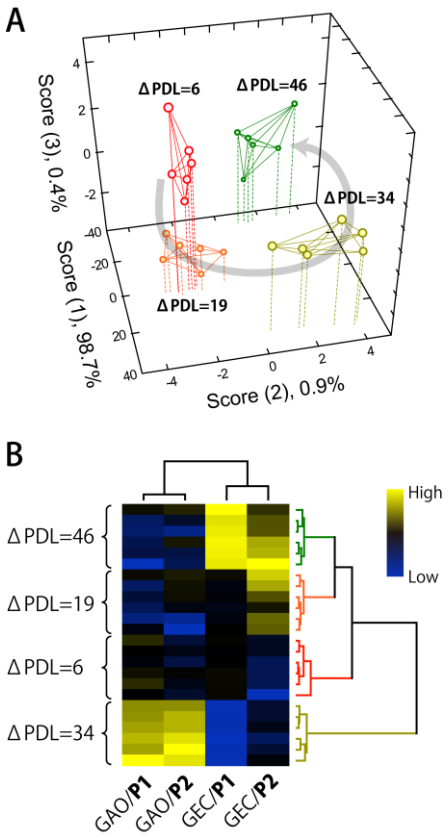

Figure 4. Analysis of the obtained fingerprints using pattern recognition methods. (A) Discriminant score plot for TIG-1 in four senescent stages obtained from the PIC array. The centers of the points that represent identical ΔPDL (same color) are connected to facilitate a visual comparison between clusters. (B) Clustering analysis of the responses obtained using the PIC array. The hierarchical clustering dendrogram based on the Euclidean distance using the Ward method was created with a data set (4 PICs × 4 ΔPDL × 6 replicates). Therein, each element was standardized prior to the analysis based on the following equation; $z = (x-\mu)/\sigma$, wherein z is the standardized score, x the raw score, μ the mean of the population, and σ the standard deviation of the population.

profiles in culture supernatants, which may contain rich information on cell states. In this manner, accurate and noninvasive sensing systems can be constructed without considering the knowledge regarding any marker molecules. Given that various senescent-inducing stimuli cause common influence on secretion profiles,[9-11] we believe that the fingerprint-based approach could provide a versatile tool for the routine monitoring of cultured cells or the screening of the influence of stimuli onto cell senescence.

ASSOCIATED CONTENT

Supporting Information

The Supporting Information is available free of charge on the ACS Publications website.

Experimental details, fingerprint profiles, statistical analysis (Tables S1-S2).

AUTHOR INFORMATION

Corresponding Author

*E-mail: s.tomita@aist.go.jp.
*E-mail: ckeitaro@mail.ecc.u-tokyo.ac.jp

Notes

The authors declare the absence of any competing financial interests.

ACKNOWLEDGMENT

This work was supported by JSPS KAKENHI grants 17H04884, 24350037, and 16K16398.

REFERENCES

(1) Loaiza, N.; Demaria, M. *Biochim. Biophys. Acta*. **2016**, *1865*, 155-167.
(2) van Deursen, J.M. *Nature* **2014,** *509*, 439-446.
(3) Childs, B.G.; Gluscevic, M.; Baker, D.J.; Laberge, R.M.; Marquess, D.; Dananberg, J.; van Deursen, J.M. *Nat. Rev. Drug Discov.* **2017,** *16*, 718-735.
(4) Debacq-Chainiaux, F.; Erusalimsky, J.D.; Campisi, J.; Toussaint, O. *Nat. Protoc.* **2009,** *4*, 1798-1806.
(5) Lee, H.W.; Heo, C.H.; Sen, D.; Byun, H.O.; Kwak, I.H.; Yoon, G.; Kim, H.M. *Anal. Chem.* **2014**, *86*, 10001-10005.
(6) Zhang, J.; Li, C.; Dutta, C.; Fang, M.; Zhang, S.; Tiwari, A.; Werner, T.; Luo, F.T.; Liu, H. *Anal. Chim. Acta.* **2017**, *968*, 97-104.
(7) Lozano-Torres, B.; Galiana, I.; Rovira, M.; Garrido, E.; Chaib, S.; Bernardos, A.; Munoz-Espin, D.; Serrano, M.; Martinez-Manez, R.; Sancenon, F. *J. Am. Chem.* Soc. **2017,** *139*, 8808-8811.
(8) Kuilman, T.; Peeper, D.S. *Nat. Rev. Cancer* **2009,** *9*, 81-94.
(9) Coppe, J.P.; Patil, C.K.; Rodier, F.; Sun, Y.; Munoz, D.P.; Goldstein, J.; Nelson, P.S.; Desprez, P.Y.; Campisi, J. *PLoS Biol*. **2008,** *6*, 2853-2868.
(10) Rodier, F.; Coppe, J.P.; Patil, C.K.; Hoeijmakers, W.A.; Munoz, D.P.; Raza, S.R.; Freund, A.; Campeau, E.; Davalos, A.R.; Campisi, J. *Nat. Cell Biol*. **2009,** *11*, 973-979.
(11) Yun, M.H.; Davaapil, H.; Brockes, J.P. *eLIFE* **2015,** *4*, e05505.
(12) Tomita, S.; Sakao, M.; Kurita, R.; Niwa, O.; Yoshimoto, K. *Chem. Sci*. **2015,** *6*, 5831-5836.
(13) Askim, J.R.; Mahmoudi, M.; Suslick, K.S. *Chem. Soc. Rev*. **2013,** *42*, 8649-8682.
(14) Chou, S.S.; De, M.; Luo, J.; Rotello, V.M.; Huang, J.; Dravid, V.P. *J. Am. Chem. Soc.* **2012,** *134*, 16725-16733.
(15) Zamora-Olivares, D.; Kaoud, T.S.; Dalby, K.N.; Anslyn, E.V. *J. Am. Chem. Soc*. **2013,** *135*, 14814-14820.
(16) Wang, M.; Ye, H.; You, L.; Chen, X. *ACS Appl. Mater. Interfaces* **2016,** *8*, 574-581.
(17) Tomita, S.; Ishihara, S.; Kurita, R. *ACS Appl. Mater. Interfaces* **2017,** *9*, 22970-22976.
(18) Tomita, S.; Matsuda, A.; Nishinami, S.; Kurita, R; Shiraki, K. *Anal. Chem.* **2017,** *89*, 7818-7822.
(19) Miranda, O.R.; Chen, H.T.; You, C.C.; Mortenson, D.E.; Yang, X.C.; Bunz, U.H.; Rotello, V.M. *J. Am. Chem. Soc*. **2010,** *132*, 5285-5289.
(20) Ran, X.; Pu, F.; Ren, J.; Qu, X. *Chem. Commun*. **2015,** *51*, 2675-2678.
(21) Tomita, S.; Niwa, O.; Kurita, R. *Anal. Chem*. **2016,** *88*, 9079-9086.
(22) Pode, Z.; Peri-Naor, R.; Georgeson, J.M.; Ilani, T.; Kiss, V.; Unger, T.; Markus, B.; Barr, H.M.; Motiei, L.; Margulies, D. *Nat. Nanotechno*l. **2017,** *12*, 1161-1168.
(23) Xu, S.; Lu, X.; Yao, C.; Huang, F.; Jiang, H.; Hua, W.; Na, N.; Liu, H.; Ouyang, J. *Anal. Chem.* **2014,** *86*, 11634-11639.
(24) Xu, S.; Wu, Y.; Sun, X.; Wang, Z.; Luo, X. *J. Mater. Chem. B* **2017,** *5*, 4207-4213.
(25) Rana, S.; Singla, A.K.; Bajaj, A.; Elci, S.G.; Miranda, O.R.; Mout, R.; Yan, B.; Jirik, F.R.; Rotello, V.M. *ACS Nano*. **2012,** *6*, 8233-8240.
(26) Le, N.D.B.; Yesilbag Tonga, G.; Mout, R.; Kim, S.T.; Wille, M.E.; Rana, S.; Dunphy, K.A.; Jerry, D.J.; Yazdani, M.; Ramanathan, R.; Rotello, C.M.; Rotello, V.M. *J. Am. Chem. Soc*. **2017,** *139*, 8008-8012.
(27) Peveler, W.J.; Yazdani, M.; Rotello, V.M. *ACS Sens.* **2016,** *1*, 1282-1285.
(28) Tomita, S.; Yoshimoto, K. *Chem. Commun.* **2013,** *49*, 10430-10432.
(29) Tomita, S.; Soejima, T.; Shiraki, K.; Yoshimoto, K. *Analyst* **2014,** *139*, 6100-6103.
(30) Kurinomaru, T.; Tomita, S.; Kudo, S.; Ganguli, S.; Nagasaki, Y.; Shiraki, K. *Langmuir* **2012,** *28*, 4334-4338.
(31) Kurinomaru, T.; Kuwada, K.; Tomita, S.; Kameda, T.; Shiraki, K. *J. Phys. Chem. B* **2017,** *121*, 6785-6791.
(32) Wadhwa, R.; Ryu, J.; Gao, R.; Choi, I.K.; Morrow, G.; Kaur, K.; Kim, I.; Kaul, S.C.; Yun, C.O.; Tanguay, R.M. *J. Biol. Chem*. **2010,** *285*, 3833-3839.
(33) Udono, M.; Kadooka, K.; Yamashita, S.; Katakura, Y. *Methods* **2012**, *56*, 383-388.
(34) Takubo, K.; Aida, J.; Izumiyama, N.; Ishikawa, N.; Fujiwara, M.; Poon, S.S.; Kondo, H.; Kammori, M.; Matsuura, M.; Sawabe, M.; Arai, T.; Baird, D.M.; Nakamura, K. *Mech. Ageing Dev.* **2010**, *131*, 614-624.
(35) Udono, M.; Fujii, K.; Harada, G.; Tsuzuki, Y.; Kadooka, K.; Zhang, P.; Fujii, H.; Amano, M.; Nishimura, S.; Tashiro, K.; Kuhara, S.; Katakura, Y. *Sci. Rep.* **2015**, *5*, 17342.
(36) Kumazaki, T.; Sakano, T.; Yoshida, T.; Hamada, K.; Sumida, H.; Teranishi, Y.; Nishiyama, M.; Mitsui, Y. *Mech. Ageing Dev.* **1998**, *101*, 91-99.
(37) Kumazaki, T.; Wadhwa, R.; Kaul, S.C.; Mitsui, Y. *Exp. Gerontol.* **1997**, *32*, 95-103.
(38) Inoue, C.; Zhao, C.; Tsuduki, Y.; Udono, M.; Wang, L.; Nomura, M.; Katakura, Y. *NPJ Aging Mech. Dis.* **2017**, *3*, 11.

Insert Table of Contents artwork here